

A Local Area Quantum Teleportation Network Based on an Array of Electrically Activated Graphene Waveguides

MUHAMMAD ASJAD,¹ MONTASIR QASYMEH,^{1,*} AND HICHEM ELEUCH^{2,3}

¹*Electrical and Computer Engineering Department, Abu Dhabi University, Abu Dhabi 59911, UAE*

²*Department of Applied Physics and Astronomy, University of Sharjah, Sharjah 27272, UAE*

³*Institute for Quantum Science and Engineering, Texas AM University, College Station, TX 77843, USA*

**montasir.qasymeh@adu.ac.ae*

Abstract: We present a scheme to generate a continuous variable (CV) multipartite entangled state using an array of plasmonic graphene waveguides that are activated by nonclassical driving microwave modes. Within this scheme, we can exploit the interaction of two light fields coupled to the same microwave mode in each waveguide to produce any type of multipartite Gaussian entangled state. A teleportation network is illustrated using the resultant CV multipartite entangled state. In particular, the proposed setup enables coherent state teleportation across remotely connected nodes with fidelity above a threshold limit of $2/3$, providing secure quantum teleportation networking even in the presence of losses.

© 2022 Optica Publishing Group under the terms of the [Optica Publishing Group Publishing Agreement](#)

1. Introduction

High-fidelity transfer of quantum states between distant nodes is key to realizing quantum networks [1–3]. However, the transfer fidelity is severely degraded by separating distances [4]. Despite the tremendous progress that has been made in developing quantum repeaters and relaying quantum information over long distances [5, 6], quantum repeaters with practical modalities have yet to be implemented [7, 8]. However, small-scale quantum networks have been realized by implementing entanglements between distant quantum nodes. For instance, short-scale quantum state transfer with moderate separation distances (a few meters) has been reported using different platforms [9, 10]. These schemes include quantum state transfer between quantum dots separated by 5 m [11], trapped atoms separated by 20 m [12], and solid-state qubits separated by 3 m [13]. Furthermore, quantum state transmission between distant microwave photons has been proposed using hybrid electro-optic entanglement [14]. We previously demonstrated quantum optical state transfer between two nodes separated by a significant distance using a microwave-enabled hybrid plasmonic graphene waveguide [15]. High-fidelity teleportation with lengths of up to 7 km was achieved using a free-space classical channel. Extending this approach to realize a quantum optical network has the potential to accomplish high-fidelity transmission among numerous nodes separated by substantial distances.

In this study, we propose the use of an array of hybrid plasmonic graphene waveguides to generate a continuous variable (CV) multipartite Gaussian Greenberger-Horne-Zeilinger (GHZ)-like entangled state between remotely connected nodes. We illustrate how the generated CV multipartite entangled states can be exploited to provide teleportation between connected plasmonic graphene waveguides. The proposed configuration incorporates N -entangled beams through N -plasmonic waveguides, which are coupled via a suitable sequence of $N - 1$ beam splitters (BSs). This result reveals that state transfer can be accomplished by performing multipartite Bell measurements on the N entangled beams. Our calculations demonstrate that a quantum state transfer can be realized within a network of up to 3 (4) nodes connected in a

star configuration with 100 (10)-m separation distances by using reasonable specifications of a free-space channel (with an attenuation of 0.005 dB/Km).

The remainder of the paper is organized as follows. In Section 2, the proposed system is described, and the governing Hamiltonian is presented. In Section 3, the equation of motion is first derived, followed by a stationary covariance matrix that describes the system stability. Multipartite entanglement is modeled and evaluated in Section 4. In Section 5, the teleportation network and numerical estimations of the transfer fidelity are discussed. Finally, conclusions are drawn in Section 6.

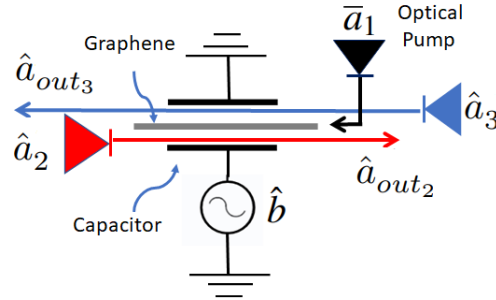


Fig. 1. The superconducting graphene-loaded capacitor driven by a nonclassical microwave field and pumped by a classical optical pump as an SPP graphene mode to compensate for losses. Two interacting quantum SPP fields counterpropagating along the graphene waveguide that are electrically coupled to the same microwave fields.

2. System

The basic building unit of the proposed system is our previously reported graphene-loaded capacitor [15–17], which consists of a graphene plasmonic waveguide integrated with a parallel-plate electrical capacitor, as illustrated in Fig 1. The operating principle of this modality is the cocoupling of two interacting quantum optical fields (for the annihilation operators \hat{a}_2 and \hat{a}_3 and frequencies ω_1 and ω_2 , respectively) that function as counter copropagating surface plasmon polariton (SPP) modes along the graphene layer. A microwave voltage (corresponding to the annihilation operator b and frequency ω_m) drives the capacitor, enabling the interaction process by electrically perturbing the graphene conductivity [18, 19]. Losses are compensated by launching a copropagating intense SPP optical pump (with an amplitude \bar{a}_1 and a frequency ω_1), and the interaction is enabled by setting $\omega_m = \omega_3 - \omega_1 = \omega_2 - \omega_2$ [20].

In this study, we consider an array (of chains) of N -independent plasmonic graphene-loaded capacitors, as shown in Fig. 2(a). The Hamiltonian of the bare system reads as follows [15]:

$$\hat{H}_0 = \sum_j^N \omega_m^j \hat{b}^{j\dagger} \hat{b} + \omega_1^j \bar{a}_1^{j*} \bar{a}_1^j + \omega_2^j \hat{a}_2^{j\dagger} \hat{a}_2^j + \omega_3^j \hat{a}_3^{j\dagger} \hat{a}_3^j, \quad (1)$$

where $j \in \{1, 2, 3, \dots, N\}$, whereas the condition $\omega_m^j = \omega_2^j - \omega_1^j = \omega_1^j - \omega_3^j$ is satisfied for every j -th element. The interaction is described by

$$\hat{H}_I = \sum_j^N g_2^j (\hat{a}_2^{j\dagger} \bar{a}_1^j \hat{b}^j + \bar{a}_1^{j*} \hat{a}_2^j \hat{b}^{j\dagger}) + g_3^j (\bar{a}_1^{j*} \hat{a}_3^j \hat{b}^j + \hat{a}_3^{j\dagger} \bar{a}_1^j \hat{b}^{j\dagger}). \quad (2)$$

Here, $g_{2,3}^j$ denotes the perturbation coupling coefficients [15].

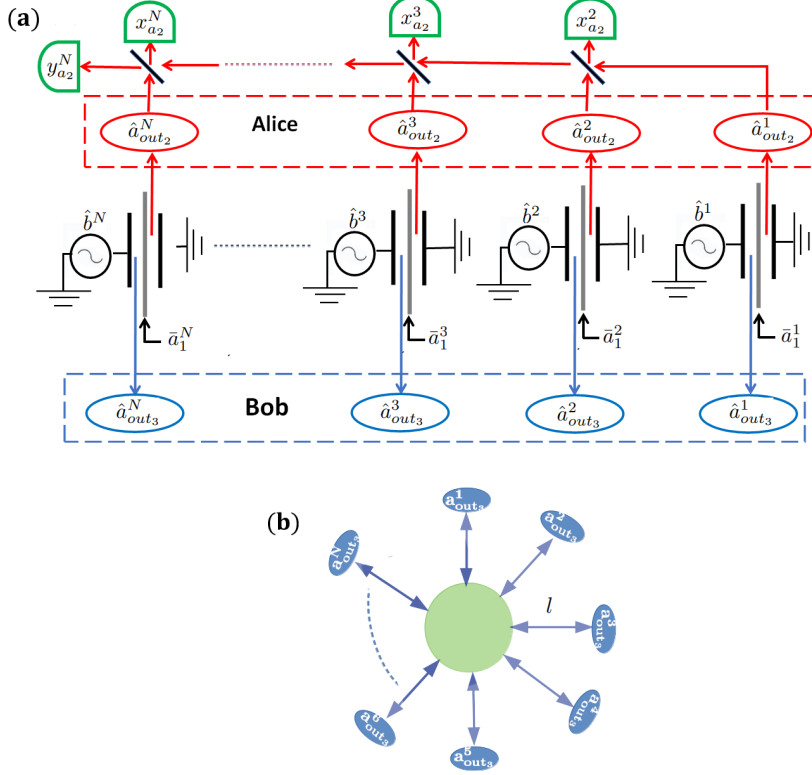


Fig. 2. (a) The structure of the proposed teleportation network composed of an array of graphene-loaded superconducting capacitors. The paired outputs of the elements (Alice and Bob modes) are processed using a system of linear optical components (beam splitters and detectors) to achieve bipartite entanglement among the Bob modes on demand. (b) An effective star-like network whereby bipartite entanglement can be produced on demand between any pair $(\hat{a}_{out3}^i, \hat{a}_{out3}^j)$ of Bob modes.

3. Equation of Motion

SPP pump modes with amplitudes \bar{a}_1^j at a frequency ω_1 are considered intense and can be treated classically. The Hamiltonian given by Eq. (1) and Eq. (2) can thus be used to obtain the equations of motion for the microwave and SPP modes of the j -th element in the context of open system dynamics under the Heisenberg-Langevin formalism given below:

$$\dot{b}^j = -\gamma_m^j b^j - i\mathcal{G}_2^j \hat{a}_2^j - i\mathcal{G}_3^j \hat{a}_3^{j\dagger} + \sqrt{2\gamma_m^j} \hat{b}_{in}^j, \quad (3)$$

$$\dot{a}_2^j = -\gamma_2^j a_2^j - i\mathcal{G}_2^j b^j + \sqrt{2\gamma_2^j} \hat{a}_{in2}^j, \quad (4)$$

$$\dot{a}_3^j = -\gamma_3^j a_3^j - i\mathcal{G}_3^j b^{j\dagger} + \sqrt{2\gamma_3^j} \hat{a}_{in3}^j, \quad (5)$$

where $\mathcal{G}_2^j = \bar{a}_1^j g_2^j$, $\mathcal{G}_3^j = \bar{a}_1^j g_3^j$, and γ_m , γ_2^j and γ_3^j are the decay rates of the microwave and SPP modes, respectively. Here, \hat{a}_{in2}^j and \hat{a}_{in3}^j are the input noise operators, characterized by $\langle \hat{a}_{in2}(t) \hat{a}_{in2}^\dagger(t') \rangle = \delta(t-t')$ and $\langle \hat{a}_{in3}(t) \hat{a}_{in3}^\dagger(t') \rangle = \delta(t-t')$, respectively. The equations in (3) to

(5) are obtained for a rotating frame at ω_m , ω_2 and ω_3 . Furthermore, we consider a nonclassical driving microwave mode with the noise operator \hat{b}_{in}^j , characterized by $\langle \hat{b}_{in}^j(t) \hat{b}_{in}^j(t') \rangle = M^j \exp^{i\phi} \delta(t - t')$ and $\langle \hat{b}_{in}^j(t) \hat{b}_{in}^{j\dagger}(t') \rangle = (N^j + 1) \delta(t - t')$. Here, M^j and N^j are expressed in terms of the *purity* \mathcal{P}^j and *nonclassicality depth* \mathcal{D}^j given below [21]:

$$M^j = \frac{1}{4\mathcal{P}^{j^2}(1 - 2\mathcal{D}^j)} - \frac{1 - 2\mathcal{D}^j}{4}, \quad (6)$$

$$N^j = \frac{1}{4\mathcal{P}^{j^2}(1 - 2\mathcal{D}^j)} + \frac{1 - 2\mathcal{D}^j}{4}. \quad (7)$$

For the sake of simplicity and without losing any generality, we assume that all microwave modes have the same *purity* $\mathcal{P}^j = \mathcal{P}$ and *nonclassicality depth* $\mathcal{D}^j = \mathcal{D}$. Consequently, and in accordance with input-output theory [22], the output field operators ($\hat{a}_{out_2}^j$ and $\hat{a}_{out_3}^j$) are related to the corresponding input operators (\hat{a}_2^j and \hat{a}_3^j) by $\hat{a}_{out_2}^j(t) = \sqrt{\gamma_2^j} \hat{a}_2^j(t) - \hat{a}_{in_2}^j(t)$ and $\hat{a}_{out_3}^j(t) = \sqrt{\gamma_3^j} \hat{a}_3^j(t) - \hat{a}_{in_3}^j(t)$, respectively. It then follows that the density matrix $\hat{\rho}_{a_2 a_3}^{out}$ of the output field modes, $\hat{\mathbf{a}}_{\mathcal{F}, out_2}(t) = (\hat{a}_{out_2}^1(t), \hat{a}_{out_2}^2(t), \dots, \hat{a}_{out_2}^N(t))$, named Alice modes, and $\hat{\mathbf{a}}_{out_3}(t) = (\hat{a}_{out_3}^1(t), \hat{a}_{out_3}^2(t), \dots, \hat{a}_{out_3}^N(t))$, named Bob modes, can be expressed as $\hat{\rho}_{a_2 a_3}^{out} = \hat{\rho}_{a_2 a_3}^{1 out} \otimes \hat{\rho}_{a_2 a_3}^{2 out}, \dots, \otimes \hat{\rho}_{a_2 a_3}^{N out}$, where

$$\hat{\rho}_{a_2 a_3}^{j out} = \int \chi_j(\varepsilon_{a_2}^j, \varepsilon_{a_3}^j) \mathcal{D}(\varepsilon_{a_2}^j) \otimes \mathcal{D}^\dagger(\varepsilon_{a_3}^j) \mathbf{d}^2 \varepsilon_{a_2}^j \mathbf{d}^2 \varepsilon_{a_3}^j. \quad (8)$$

Here, $\mathcal{D}(\varepsilon_{a_2}^j) = \exp(\varepsilon_{a_2}^j \hat{a}_{out_2}^{j\dagger} - \varepsilon_{a_2}^{j*} \hat{a}_{out_2}^j)$ and $\mathcal{D}(\varepsilon_{a_3}^j) = \exp(\varepsilon_{a_3}^j \hat{a}_{out_3}^{j\dagger} - \varepsilon_{a_3}^{j*} \hat{a}_{out_3}^j)$ are the displacement operators for the j -th Alice and Bob modes, respectively. The complex phase-space variables $\varepsilon_{a_2}^j = (x_{a_2}^j + iy_{a_2}^j)/\sqrt{2}$ and $\varepsilon_{a_3}^j = (x_{a_3}^j + iy_{a_3}^j)/\sqrt{2}$ correspond to the bosonic operators $\hat{a}_{out_2}^j = (\hat{x}_{a_2}^j + i\hat{y}_{a_2}^j)/\sqrt{2}$ and $\hat{a}_{out_3}^j = (\hat{x}_{a_3}^j + i\hat{y}_{a_3}^j)/\sqrt{2}$, respectively. The real phase-space variables $x_{a_2}^j$ ($x_{a_3}^j$) and $y_{a_2}^j$ ($y_{a_3}^j$) are the counterparts of the Hermitian quadrature operators $\hat{x}_{a_2}^j$ ($\hat{x}_{a_3}^j$) and $\hat{y}_{a_2}^j$ ($\hat{y}_{a_3}^j$), respectively. Furthermore, $\chi(\varepsilon_{a_2}, \varepsilon_{a_3})$ is the characteristic function, which is the Fourier transform of the Wigner function, i.e., $\chi(\varepsilon_{a_2}, \varepsilon_{a_3}) = \mathcal{F}[\mathcal{W}(\varepsilon_{a_2}, \varepsilon_{a_3})]$. The joint Wigner function for $2N$ output modes can be formalized for zero-mean Gaussian quantum states as

$$\mathcal{W}(\mathbf{r}_{a_2}, \mathbf{r}_{a_3}) = \mathcal{N}_r \exp \left\{ -\frac{1}{2} (\mathbf{r}_{a_2}, \mathbf{r}_{a_3}) \mathcal{V}^{-1} (\mathbf{r}_{a_2}, \mathbf{r}_{a_3})^T \right\}, \quad (9)$$

where \mathcal{N}_r is the normalization factor, the subscript T denotes the transpose, $\mathbf{r}_{a_2} = (x_{a_2}^1, y_{a_2}^1, x_{a_2}^2, y_{a_2}^2, \dots, x_{a_2}^N, y_{a_2}^N)$ and $\mathbf{r}_{a_3} = (x_{a_3}^1, y_{a_3}^1, x_{a_3}^2, y_{a_3}^2, \dots, x_{a_3}^N, y_{a_3}^N)$ are the vectors of the real variables associated with the Alice and Bob modes, and \mathcal{V} is the $4N \times 4N$ covariance matrix (CM), which can be written in the following block form:

$$\mathcal{V} = \begin{pmatrix} \mathcal{V}_{a_2} \mathcal{I}_{2N} & \mathcal{V}_{a_2 a_3} \mathcal{I}_{2N} \\ \mathcal{V}_{a_2 a_3}^T \mathcal{I}_{2N} & \mathcal{V}_{a_3} \mathcal{I}_{2N} \end{pmatrix}. \quad (10)$$

Here, $\mathcal{V}_{a_2} = \text{diag}(\mathcal{V}_{a_2}^1, \mathcal{V}_{a_2}^2, \mathcal{V}_{a_2}^3, \dots, \mathcal{V}_{a_2}^N)$ and $\mathcal{V}_{a_3} = \text{diag}(\mathcal{V}_{a_3}^1, \mathcal{V}_{a_3}^2, \dots, \mathcal{V}_{a_3}^N)$ are the $2N \times 2N$ covariance matrices for the Alice and Bob modes, respectively. Additionally, $\mathcal{V}_{a_2 a_3}$ is a $2N \times 2N$ matrix that describes the correlation between the Alice (\hat{r}_a) and Bob (\hat{r}_{a_3}) modes. The stationary covariance matrix \mathcal{V}^j for the j -th pair of Alice and Bob modes is given by

$$\mathcal{V}^j = \int_{-\infty}^{\infty} Q^j \mathcal{T}^j(\omega) \mathcal{N}_{in}^j \mathcal{T}^{jT}(-\omega) Q^{jT} d\omega, \quad (11)$$

where $\mathcal{N}_{in}^j = \text{diag}(\mathcal{N}_2^j, \mathcal{N}_3^j, \mathcal{N}_b^j)$ is the diffusion matrix, $\mathcal{N}_2^j = \mathcal{N}_3^j = \begin{pmatrix} 0 & 1 \\ 0 & 0 \end{pmatrix}$, $\mathcal{Q}^j = \text{diag}(\mathcal{Q}_2^j, \mathcal{Q}_3^j, \mathcal{Q}_b^j)$,

$\mathcal{Q}_3^j = \frac{1}{2} \begin{pmatrix} 1 & 1 \\ -i & -i \end{pmatrix}$, and $\mathcal{N}_b^j = \begin{pmatrix} M^j & N^j + 1 \\ N_m^j & M^* \end{pmatrix}$. Here, $\mathcal{T}^j(\omega) = F^j(\omega)[\mathcal{A}^j - i\omega]^{-1}\nu^j - \mathbf{I}$, $\nu = \text{diag}(\sqrt{2\gamma_2^j}, \sqrt{2\gamma_2^j}, \sqrt{2\gamma_3^j}, \sqrt{2\gamma_3^j}, \sqrt{2\gamma_m^j}, \sqrt{2\gamma_m^j})$, $F^j(\omega) = \text{diag}(\sqrt{2\gamma_2^j}, \sqrt{2\gamma_2^j}, \sqrt{2\gamma_3^j}, \sqrt{2\gamma_3^j}, 1, 1)$, and the drift matrix for the j -th element in the \mathcal{A}^j array is given by

$$\mathcal{A}^j = \begin{pmatrix} -\gamma_2^j & 0 & 0 & 0 & -i\mathcal{G}_2^j & 0 \\ 0 & -\gamma_2^j & 0 & 0 & 0 & i\mathcal{G}_2^j \\ 0 & 0 & -\gamma_3^j & 0 & 0 & -i\mathcal{G}_3^j \\ 0 & 0 & 0 & -\gamma_3^j & i\mathcal{G}_3^j & 0 \\ -i\mathcal{G}_2^j & 0 & 0 & -i\mathcal{G}_3^j & -\gamma_m^j & 0 \\ 0 & i\mathcal{G}_2^j & i\mathcal{G}_3^j & 0 & 0 & -\gamma_m^j \end{pmatrix}. \quad (12)$$

According to the Routh-Hurwitz criterion [23], the stability of the steady-state solution can be guaranteed if the real part of the eigenvalues of \mathcal{A}^j are negative. In this work, proper parameters are considered to attain stable solutions (see the stability analysis in the Appendix).

4. Multipartite Entanglement

In this section, we show how N -distant independent plasmonic graphene waveguides can be used to generate an N -partite CV entangled state. This system can be realized by sending the output of the Alice modes ($\hat{a}_{out_2}^j$) from each plasmonic graphene waveguide to an intermediate conman node (named Charlie), where multipartite Bell measurement is performed. An N -partite entangled state of the Bob modes ($\hat{a}_{out_3}^j$) is thus prepared. As shown in Fig. 2(a), Charlie combines the Alice modes on an array of $N - 1$ beam splitters (BS) with respective ratios of 1:1, 1:2, ..., 1 : $N-1$ and then performs multipartite homodyne detection on the BS output fields. The classical result \bar{r}_a is generated. Accordingly, the transformed position (phase) quadratures of the Alice modes are given by

$$\hat{x}_{a_2}^1 \rightarrow \sum_j^N \hat{x}_{a_2}^j / \sqrt{N} \quad (\hat{y}_{a_2}^1 \rightarrow \sum_j^N \hat{y}_{a_2}^j / \sqrt{N}), \quad (13)$$

$$\begin{aligned} \hat{x}_{a_2}^{N-1} &\rightarrow \left(\sum_j^{N-1} \hat{x}_{a_2}^j - (N-1)\hat{x}_{a_2}^N \right) / \sqrt{N(N-1)} \\ \hat{y}_{a_2}^{N-1} &\rightarrow \left(\sum_j^{N-1} \hat{y}_{a_2}^j - (N-1)\hat{y}_{a_2}^N \right) / \sqrt{N(N-1)}. \end{aligned} \quad (14)$$

Note that the first $N - 1$ outputs $\hat{a}_{\mathcal{F},out_2}^j$ (with $j = 1, 2, 3, \dots, N - 1$) in the multipartite Bell measurement of the Alice modes are homodyne when detected in the position quadrature $\hat{x}_{a_2}^j$, whereas the last output $\hat{a}_{\mathcal{F},out_2}^N$ is detected in the phase quadrature $\hat{y}_{a_2}^N$. As a result, all the Bob modes can be efficiently driven into an N -partite entangled state. The corresponding Wigner

function of the conditioned Bob' modes for the detection result $\bar{\mathbf{r}}_a$ reads

$$W(\mathbf{r}_b/\bar{\mathbf{r}}_a) = \mathcal{N}' \exp \left\{ -\frac{1}{2} \mathbf{r}_b \mathcal{V}'^{-1} \mathbf{r}_b^T \right\}, \quad (15)$$

where \mathcal{V}' is a $2N \times 2N$ covariance matrix that describes the N-partite entangled Gaussian state. Note that first-order terms are not shown in Eq. (15) because these terms have a negligible impact and can be zeroed by considering appropriate feedback. The covariance matrix \mathcal{V}' for N-identical plasmonic graphene waveguides ($\mathcal{V}_{a_2^j} = \mathcal{V}_a$, $\mathcal{V}_{a_3^j} = \mathcal{V}_{a_3}$ and $\mathcal{V}_{a_2^j a_3^j} = \mathcal{V}_{a_2 a_3}$) can be written in the following block form:

$$\mathcal{V}' = \begin{pmatrix} \mathcal{V}'_{a_3} & \mathcal{V}'_{a_3 a_3} & \cdots & \mathcal{V}'_{a_3 a_3} \\ \mathcal{V}'_{a_3 a_3} & \mathcal{V}'_{a_3} & & \mathcal{V}'_{a_3 a_3} \\ \vdots & & \ddots & \vdots \\ \mathcal{V}'_{a_3 a_3} & \cdots & \mathcal{V}'_{a_3 a_3} & \mathcal{V}'_{a_3} \end{pmatrix}, \quad (16)$$

where $\mathcal{V}'_{a_3} = \mathcal{V}_{a_3} - (N-1)\mathcal{V}_{a_2 a_3}\mathcal{Z}_1\mathcal{V}_{a_2}^{-1}\mathcal{Z}_1\mathcal{V}_{a_2 a_3}/N - \mathcal{V}_{a_2 a_3}\mathcal{Z}_2\mathcal{V}_{a_2}^{-1}\mathcal{Z}_2\mathcal{V}_{a_2 a_3}/N$ and $\mathcal{V}'_{a_3 a_3} = \mathcal{V}_{a_2 a_3}\mathcal{Z}_1\mathcal{V}_{a_2}^{-1}\mathcal{Z}_1\mathcal{V}_{a_2 a_3}/N - \mathcal{V}_{a_3 a_3}\mathcal{Z}_2\mathcal{V}_{a_2}^{-1}\mathcal{Z}_2\mathcal{V}_{a_2 a_3}/N$ are 2×2 submatrices with $\mathcal{Z}_1 = \text{diag}(1, 0)$ and $\mathcal{Z}_2 = \text{diag}(0, 1)$.

The stationary entanglement between any pair of Bob modes can be measured by the logarithmic negativity [24, 25]:

$$E_N^{(j)} = \max [0, -\ln 2\eta_j^-], \quad (17)$$

where η_j^- is the smallest symplectic eigenvalue of the partially transposed covariance matrix \mathcal{V}'^j of the j -th pair of Bob modes. A nonzero value of $E_N^{(j)}$ can be used to quantify the degree of entanglement between the j -th pair of Bob modes.

The N-partite stationary entanglement at the output can be exploited to realize a quantum network. The channel- and transmission-associated losses can be described using the concept of an effective beam splitter with a transmissivity $\eta = \eta_0 e^{-\alpha l/10}$ [26], where α is the classical channel attenuation in dB/km , η_0 describes all possible inefficiencies, and l is the distance traveled by each field (the classical channel length) [27, 28]. It then follows that the corresponding output covariance matrix is given by $\mathcal{V}'_{los} = \eta \mathcal{V}' + \frac{1}{2}(1-\eta)\mathbf{I}$, where \mathbf{I} is the $2N \times 2N$ identity matrix. Here, all the Bob modes are assumed to be equidistant from the central hub (i.e., l).

Fig. (3) shows the calculated logarithmic negativity for the proposed scheme versus the number of Bob modes (the number of independent plasmonic waveguides). The calculations are performed for different degrees of nonclassicality of the driving microwave field. Additionally, the simulations are performed in the absence and presence of losses, as shown in Fig. 3(a) and Fig. 3(b), respectively. The nonclassicality associated with the microwave field enables an increase in the entanglement between any pair of Bob modes (red squares). For instance, for the parameters considered in Fig. (3) of $\gamma_1/\omega_m = 0.001$, $\gamma_2/\omega_m = \gamma_3/\omega_m = 0.02$, $\mathcal{G}_2/\omega_m = 0.2$, $\mathcal{G}_3/\omega_m = 0.16$, $\eta_0 = 0.99$ and $l = 0.1 km$ and $\alpha = 0.005$, our numerical investigations show that the logarithmic negativity is maximally boosted for $\mathcal{D} = 0.494$. However, when the number of Bob modes increases, the logarithmic negativity becomes more sensitive (degrades). Our simulations show that incorporating the nonclassicality of the driving microwave field results in a logarithmic negativity greater than zero for up to 10 Bob modes with separation distances of approximately 0.1 km. Hence, it is demonstrated that Charlie can generate any type of entangled state among different numbers of Bob modes by choosing a proper array of BSs.

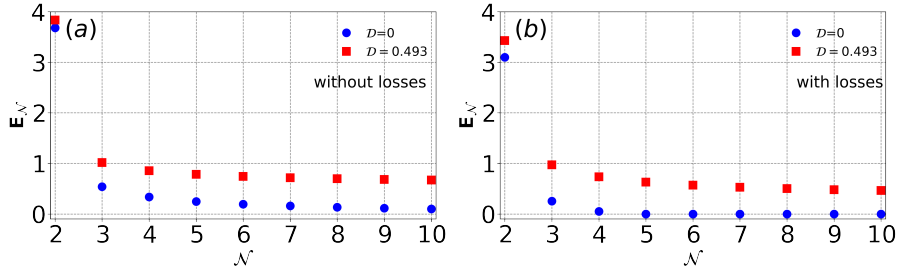


Fig. 3. Logarithmic negativity E_N between any pair of Bob modes as a function of the number of modes N in the limit of zero bandwidth. Two cases of nonclassical depth $\mathcal{D} = 0$ (blue dots) and $\mathcal{D} = 0.493$ (red squares) are considered. In (a), losses are neglected, whereas in (b), a realistic channel of free space (with $\alpha = 0.005$) and a detection efficiency $\eta_0 = 99\%$ are considered. The other parameters are $\gamma_m/\omega_m = 0.001$, $\gamma_2/\omega_m = \gamma_3/\omega_m = 0.02$, $\mathcal{G}_2/\omega_m = 0.2$, $\mathcal{G}_3/\omega_m = 0.16$, and $l = 0.1\text{km}$.

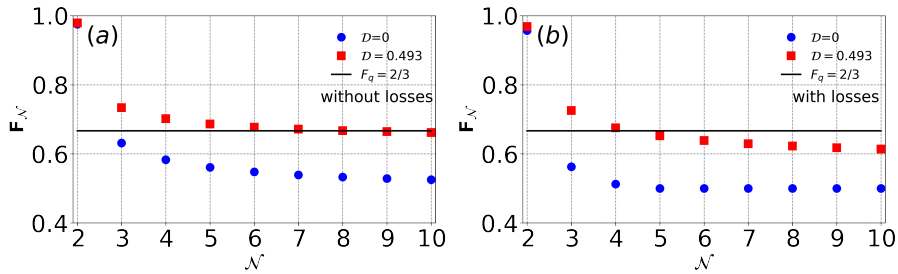


Fig. 4. Optimal teleportation fidelity F_N as a function of the number of Bob modes. All parameters are the same as those shown in Fig. (3). The horizontal black line corresponds to the secure quantum teleportation threshold $F_q = 2/3$.

5. Teleportation Network

The output N -partite Gaussian entangled states can be characterized and function as a quantum channel for multipartite quantum teleportation. To this end, we analyze the performance of this multipartite quantum channel realized by the Bell measurements in terms of the teleportation fidelity of a pure coherent state among the Bob modes ($\hat{a}_3^1, \hat{a}_3^2, \hat{a}_3^3, \dots, \hat{a}_3^N$). Therefore, for CV teleportation protocols, Bob combines an unknown input coherent state $|\alpha_{in}\rangle$ (that is to be teleported) with the part of the entangled state in his hand, \hat{a}_3^1 , on a beam splitter and measures two quadratures $1/\sqrt{2}(\hat{x}_{in} - \hat{x}_{a_3}^1)$ and $1/i\sqrt{2}(\hat{p}_{in} - \hat{p}_{a_3}^1)$, where $\alpha_{in} = (\hat{x}_{in} + i\hat{p}_{in})/\sqrt{2}$. The measurement outcomes are sent to $N - 1$ receivers simultaneously. Each of the $N - 1$ Bob modes displaces its state according to the measurement outcomes. The corresponding optimal teleportation fidelity is given by [29]

$$F_{a_3^1:a_3^j} = \frac{1}{1 + 2\eta_j^-}, \quad (18)$$

where η_j^- is equivalent to the smallest symplectic eigenvalue of the partially transposed \mathcal{V}' under the bipartition $a_3^1 : a_3^2 a_3^3 \cdots a_3^{N-1}$. The optimal fidelity is directly related to the logarithmic negativity $E_N^{(n)}$.

In Fig. (4), the optimal teleportation fidelity F_N of the unknown coherent state is calculated as

a function of the number of Bob modes. Here, zero and $\mathcal{D} = 0.494$ nonclassicality depths are considered. Additionally, the cases of lossless and realistic free space channels are evaluated in Fig. 4(a) and Fig. 4(b), respectively. The calculations show that the nonclassicality of the driving microwave field enables the threshold for a secure quantum teleportation limit $F_q = 2/3$ (the black horizontal line) to be exceeded, even in the presence of losses. However, our simulations show that up to only four Bob modes have fidelity beyond the threshold.

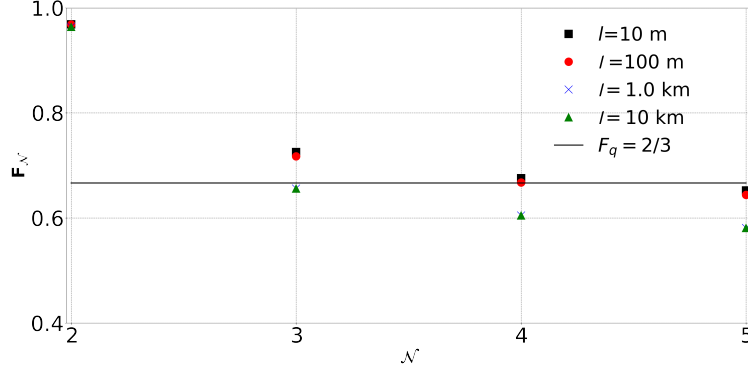


Fig. 5. Optimal teleportation fidelity F_N as a function of the number of Bob modes. Different values of the distance $l=0$ km (black), 0.1 km (red), 1.0 km (blue), 5.0 km (green) and 9.0 km (magenta) are considered. The optimal nonclassicality depth $\mathcal{D} = 0.494$ and all other parameters are the same as those shown in Fig. (3). The horizontal black line corresponds to the secure quantum teleportation threshold $F_q = 2/3$.

Fig. (5) shows the robustness of the teleportation fidelity versus the number of Bob modes N for different values of the separation distance l . Here, $\mathcal{D} = 0.494$, realistic free space channel losses are taken into account, and all other parameters are the same as those shown in Fig. (3). Interestingly, the teleportation fidelity can bear the required quantum threshold for $l = 0.1\text{ km}$ and $N = 3$ or alternatively for $l = 10\text{ m}$ and $N = 4$. As a consequence, there is a trade-off between the separation distance and the number of Bob modes. This very promising result shows how a quantum teleportation network can be realized.

6. Conclusion

We have presented a novel scheme for generating multipartite continuous-variable entangled states among remotely connected independent nodes. The proposed system employs an array of separated graphene plasmonic waveguides that are activated by biasing nonclassical microwave drivers to produce an array of light beams with a multipartite entangled state. We have demonstrated that the resulting multipartite entanglement can be exploited to implement a quantum network. Furthermore, we have proven that in the presence of nonclassical driving microwave modes, teleportation between any pair of network nodes can be accomplished with a fidelity greater than the quantum threshold, enabling secure communication even in the presence of losses. The proposed scheme is a demonstration of a secure teleportation network implementing realistic lossy channels.

Appendix

Following the Routh-Hurwitz criterion, the steady-state stability conditions derived from \mathcal{A}^j in E.q. (10) are given by:

$$\begin{aligned} S_1 &= \gamma_m^j + \gamma_2^j + \gamma_3^j > 0, \\ S_2 &= \gamma_m^j + \mathcal{G}_2^{j^2} / \gamma_2^j - \mathcal{G}_3^{j^2} / \gamma_3^j > 0, \\ S_3 &= \gamma_2^j + \gamma_3^j + \frac{\mathcal{G}_2^{j^2}}{\gamma_m^j + \gamma_3^j} - \frac{\mathcal{G}_3^{j^2}}{\gamma_m^j + \gamma_2^j} > 0. \end{aligned} \quad (19)$$

In Fig. (6), we evaluate the stability parameters S_1 , S_2 and S_3 against \mathcal{G}_3/ω_m while considering all parameters same as in Fig.(3). The simulations in Fig.6 show that the stability conditions are satisfied for $\mathcal{G}_3/\omega_m < 0.2$. Hence, the considered parameters in this work, including $\mathcal{G}_3/\omega_m = 0.16$, are corresponding to stable steady-state case.

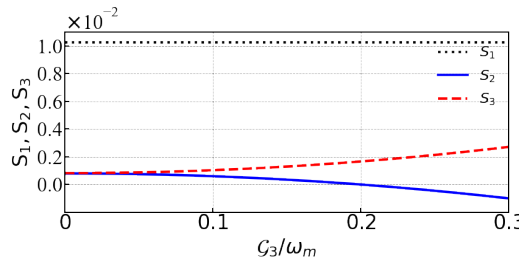


Fig. 6. Stability conditions S_1 , S_2 and S_3 as a function of the effective coupling \mathcal{G}_3/ω_m for all parameters same as in Fig.(3).

Data Availability - The data sets generated and/or analysed during the current study are available from the corresponding author on reasonable request.

Acknowledgments - This research is supported by Abu Dhabi Award for Research Excellence under ASPIRE/Advanced Technology Research Council (AARE19-062) 2019.

Competing Interests - The authors declare that there are no competing interests.

Correspondence - Correspondence and requests for materials should be addressed to M.Q. (email: montasir.qasymeh@adu.ac.ae).

References

1. J. I. Cirac, P. Zoller, H. J. Kimble, and H. Mabuchi, "Quantum state transfer and entanglement distribution among distant nodes in a quantum network," *Phys. Rev. Lett.* **78**, 3221–3224 (1997).
2. H. J. Kimble, "The quantum internet," *Nature* **453**, 1023–1030 (2008).
3. S. Wehner, D. Elkouss, R. Hanson, "Quantum internet: A vision for the road ahead," *Science* **362**, 6412 (2018).
4. L.-M. Duan, M.D. Lukin, J. I. Cirac and P. Zoller, "Long-distance quantum communication with atomic ensembles and linear optics" *Nature* **414**, 413–418 (2001).
5. H. J. Kimble, "The quantum internet," *Nature* **453**, 1023–1030 (2008).
6. K. Azuma, K. Tamaki, and H.-K. Lo, "All-photonic quantum repeaters," *Nature Comm.* **6**, 6787 (2015).
7. L. Gyongyosi and S. Imre, "Resource prioritization and balancing for the quantum internet" *Sci. Rep.* **10**, 22390 (2020).
8. M. Ruf, N. H. Wan, H. Choi, D. Englund, and R. Hanson, "Quantum networks based on color centers in diamond," *J. Appl. Phys.* **130**, 070901 (2021).
9. C. Cabrillo, J. I. Cirac, P. Garcia-Fernandez, and P. Zoller, "Creation of entangled states of distant atoms by interference," *Phys. Rev. A* **59**, 2 (1999).

10. M. M. Weston, S. Slussarenko, H. M. Chrzanowski, S. Wollmann, L. K. Shalm, V. B. Verma, M. Allman, S. W. Nam, and G. J. Pryde, "Heralded quantum steering over a high-loss channel," *Science Advances* **4**, 1 (2018).
11. A. Delteil, G. Sun, W.-b. Gao, E. Togan, S. Faelt and A. Imamoglu, "Generation of heralded entanglement between distant hole spins," *Nature Phys.* **12**, 218–223 (2016).
12. J. Hofmann, M. Krug, N. Ortegel, L. Gérard, M. Weber, W. Rosenfeld, and H. Weinfurter, "Heralded Entanglement Between Widely Separated Atoms," *Science* **337**, 72-75 (2012).
13. H. Bernien, B. Hensen, W. Pfaff, G. Koolstra, M. S. Blok, L. Robledo, T. H. Taminiau, M. Markham, D. J. Twitchen, L. Childress and R. Hanson, "Heralded entanglement between solid-state qubits separated by three metres," *Nature* **497**, 86–90 (2013).
14. S. Krastanov, H. Raniwala, J. Holzgrafe, K. Jacobs, M. Loncar, M. J. Reagor, and D. R. Englund, "Optically Heralded Entanglement of Superconducting Systems in Quantum Networks," *Phys. Rev. Lett.* **127**, 040503 (2021).
15. M. Asjad, M. Qasymeh, H. Eleuch , "Continuous-Variable Quantum Teleportation Using Microwave Enabled Plasmonic Graphene Waveguide" *Phys. Rev. Applied* **16**, 034046, (2021).
16. M. Qasymeh and H. Eleuch , "Entanglement of Microwave and Optical Fields using Electrical Capacitor Loaded with Plasmonic Graphene Waveguide," *IEEE Photonics*, **12** Art. no. 7500212, (2020).
17. M. Qasymeh and H. El Euch , "Wideband Graphene-Based Electro-Optic Entangler," U.S. Patent, No. 11048107, (2021).
18. M. Qasymeh and H. Elruch , "Quantum Microwave-to-Optical Conversion in Electrically Driven Multilayer Graphene," *Optics Express*, **27**, 5945-5960, (2019).
19. M. Qasymeh and H. El Euch , "Frequency-Tunable Quantum Microwave to Optical Conversion System," U.S. Patent, No. 10,824,048 B2, (2020).
20. M. Qasymeh and H. Eleuch , "Hybrid Two-Mode Squeezing of Microwave and Optical Fields Using Optically Pumped Graphene Layers," *Scientific Reports*, **10**, 16676, (2020).
21. R. Tahiria, M. Ikram, H. Nha and M. S. Zubairy, "Entanglement of Gaussian states using a beam splitter," *Phys. Rev.A* **79**, 023816 (2009)
22. C. W. Gardiner and M. J. Collett, "Input and output in damped quantum systems: Quantum stochastic differential equations and the master equation," *Phys. Rev. A* **31**, 3761 (1985).
23. E. X. DeJesus and C. Kaufman, "Routh-Hurwitz criterion in the examination of eigenvalues of a system of nonlinear ordinary differential equations," *Phys. Rev. A* **35**, 5288 (1987).
24. M.B. Plenio. "The logarithmic negativity: A full entanglement monotone that is not convex," *Phys. Rev. Lett.* **95**, 090503 (2005).
25. G. Vidal and R. F. Werner, "Computable measure of entanglement," *Phys. Rev. A* **65**, 032314 (2002).
26. F. A. S. Barbosa, A. J. de Faria, A. S. Coelho, K. N. Cassemiro, A. S. Villar, P. Nussenzveig, and M. Martinelli, "Disentanglement in bipartite continuous-variable systems, *Phys. Rev. A* **84**, 052330 (2011).
27. M. Asjad, P. Tombesi and D. Vitali, "Feedback control of two-mode output entanglement and steering in cavity optomechanics," *Phys. Rev. A* **94**, 052312 (2016).
28. M. Asjad, S. Zippilli, P. Tombesi and D. Vitali, "Large distance continuous variable communication with concatenated swaps," *Physica Scripta* **90** 074055 (2015).
29. A. Mari, and D. Vitali, "Optimal fidelity of teleportation of coherent states and entanglement," *Phys. Rev. A* **78**, 062340 (2008).